

Exploring the origin of stars on bound and unbound orbits causing tidal disruption events

Shiyan Zhong¹, Kimitake Hayasaki², Shuo Li³, Peter Berczik^{3,4,5}, Rainer Spurzem^{4,5,6,†}

Received _____; accepted _____

¹Yunnan Observatories, Chinese Academy of Sciences, 396 Yang-Fang-Wang, Guandu District, 650216, Kunming, Yunnan, China

²Department of Astronomy and Space Science, Chungbuk National University, Cheongju 361-763, Korea

³National Astronomical Observatories of China, Chinese Academy of Sciences, 20A Datun Rd., Chaoyang District, 100012, Beijing, China

⁴Main Astronomical Observatory, National Academy of Sciences of Ukraine, 27 Akademika Zabolotnoho St., 03680, Kyiv, Ukraine

⁵Astronomisches Rechen-Institut, Zentrum für Astronomie, University of Heidelberg, Mönchhofstrasse 12-14, 69120, Heidelberg, Germany

⁶Kavli Institute for Astronomy and Astrophysics, Peking University, Beijing, China

[†]Research Fellow at Frankfurt Institute for Advanced Studies

Abstract

Tidal disruption events (TDEs) probe properties of supermassive black holes (SMBHs), their accretion disks, and the surrounding nuclear stellar cluster. Light curves of TDEs are related to orbital properties of stars falling SMBHs. We study the origin, density, and velocity distributions of bound and unbound stars in the nuclear star cluster, which are causing TDEs as a function of their orbital eccentricity e and energy E . These quantities determine near the SMBH the ratio of the orbit's pericenter to tidal disruption radii (denoted as penetration factor β). We develop an analytical model for the density and velocity distribution of such stars in the cluster, which agrees well with N -body experiments. Our model extends classical models of angular momentum diffusion in the loss cone. We also derive an analytical model for three characteristic eccentricities in the loss cone: the minimum and maximum value for given β , respectively, and e_{lcb} , which represents the orbital eccentricity defining the boundary between empty and full loss cone regimes. With N -body experiments, we show that stars causing TDEs are distributed between these eccentricity limits on the $e - \beta$ plane. Moreover, we find most of the bound stars between e_{lcb} and $e = 1$ (i.e., the full loss cone regime), whereas the remaining bound stars are originating from the empty loss cone regime. This is consistent with the loss cone theory. We propose that the $e - \beta$ distribution of stars in a star cluster or galactic nucleus can be a good tool to diagnose whether the stars can cause TDEs.

Subject headings: galaxies: kinematics and dynamics – galaxies: nuclei – methods: numerical – quasars: supermassive black holes – stars: kinematics and dynamics

1. Introduction

Most galaxies harbor supermassive black holes (SMBHs) with million to billion solar masses at their center. Tidal disruption events (TDEs) provides a good opportunity to identify dormant SMBHs in inactive galaxies. A star approaching the SMBH is tidally destroyed, once it enters the tidal disruption radius, where the star is torn apart by the black hole tidal force (Hills 1975). Mainly because the fallback material accretes onto the SMBH, a flaring event occurs with large luminosity and a duration of months to years (Rees 1988).

In the classical TDE theory, the star approaches the SMBH on a parabolic orbit (i.e., $e = 1$, where e is the orbital eccentricity.) and is tidally disrupted at $r_t = (M_{\text{BH}}/m_*)^{1/3}r_*$, where M_{BH} , m_* , and r_* are the black hole mass, stellar mass and radius, respectively. After disruption, a half of the stellar debris is gravitationally bound and falls back to the SMBH at a rate being proportional to $-5/3$ power of time because of the Kepler’s third law, and thus the bolometric luminosity is proportional to $t^{-5/3}$ (Evans & Kochanek 1989; Phinney 1989). However, recent observations have revealed that some observed TDEs show light curves, which deviate from the $t^{-5/3}$ decay rate (Gezari et al. 2012; Holoien et al. 2014; Gezari et al. 2015; Miller et al. 2015; Holoien et al. 2016; van Velzen et al. 2019). Dozens of X-ray TDEs have light curves shallower than $t^{-5/3}$ (Auchettl et al. 2017), while many optical/UV TDEs are well fit by $t^{-5/3}$ (e.g. Hung et al. 2017).

Lodato & Rossi (2011) have shown that the luminosity of the accretion disk observed in different bands may decay with diverse power-law indexes. For TDEs with the well-evolved optically thick disks, the observed X-ray light curves should decay following the form of a power-law multiplied by an exponential, which is caused by the Wien tail of the disk spectrum (Mummery & Balbus 2020). Moreover, when mass falls back to the SMBH at super-Eddington rate, an outflow could be launched from the accretion disk. The luminosity

of the outflow can decay with time more shallowly than $t^{-5/3}$ (Strubbe & Quataert 2009). The mass fallback rate can deviate from the $t^{-5/3}$ decay rate because of the orbital eccentricity (Hayasaki et al. 2013, 2018; Park & Hayasaki 2020), the survived core through partial tidal disruption (Guillochon & Ramirez-Ruiz 2013), the stellar internal structure (Lodato et al. 2009; MacLeod et al. 2012), and the penetration factor $\beta = r_t/r_p$ (Park & Hayasaki 2020), where r_p is the pericenter distance radius.

Hayasaki et al. (2018) have examined the stellar distribution of a spherical stellar cluster on the e - β plane for a given number of particles and tidal disruption radius by N -body experiments. They found that there are two interesting features: first, there are two critical values of the orbital eccentricity as a function of M_{BH}/m_* and β , indicating the distribution of e is coupled with the distribution of β . The light curve characteristics of tidal disruption flares are divided by the two critical eccentricities (see also Park & Hayasaki 2020). Second, the valid region of the stars causing TDEs is constrained to a certain part of the e - β plane. Although the orbital eccentricity and the penetration factor are important parameters to characterize the TDE flare, little has been known how these orbital parameters are related to the stellar distribution and dynamics in a spherical star cluster.

In this paper, we analytically derive the number densities of the bound and unbound stars, which can cause TDEs, in a spherical cluster and test them by performing N -body simulations. We also examine the distribution of the stars on the e - β plane. We construct our analytical models in Section 2, and then describe the detail of N -body simulations in Section 3. We discuss our results in Section 4 and draw our conclusions in Section 5.

2. Orbital parameter dependence of the stellar distribution

We first briefly review the theory of the stellar number density in a spherical star cluster, which is proposed by Cohn & Kulsrud (1978) (hereafter CK78). Then we derive the number densities of the stars on bound and unbound orbits based on the CK78 solution. In what follows, we use subscript ‘b’ and ‘u’ to mark the quantities corresponding to bound and unbound cases, respectively.

2.1. Stellar distributions in the energy-angular momentum phase space

When an SMBH resides in the center of a star cluster, a stellar cusp forms within an influence radius of the SMBH, r_h . A stellar orbit can be determined by both the specific orbital energy of a star: $E = v^2/2 - GM_{\text{BH}}/r$ and the normalized squared angular momentum of the star:

$$\mathcal{R} = \left(\frac{J}{J_c} \right)^2, \quad (1)$$

where v , G , J and J_c are the velocity of the star, gravitation constant, specific angular momentum of the star and the corresponding circular angular momentum, respectively. In the spherically symmetric cusp with isotropic velocity dispersion, the number density distribution of the stars simply depends on the orbital energy. However, the isotropic velocity distribution breaks down because the SMBH removes the stars with low angular momentum through TDEs. In the classical loss cone theory, the number density should also depend on \mathcal{R} , and thus should be a function of both E and \mathcal{R} as $n(\mathcal{R}, E)$ (Frank & Rees 1976). In phase space the loss cone region is encompassed by \mathcal{R}_{lc} , where \mathcal{R}_{lc} is the square of the normalized loss cone angular momentum (see equation 12). The stars inside the loss cone region can survive for no more than one orbital period, unless they find a way out before being disrupted. Thus the loss cone runs out of stars quickly and $n(\mathcal{R}, E)$ vanishes to

zero at $\mathcal{R} < \mathcal{R}_{\text{lc}}$. On the other hand, two-body encounters can replenish continuously new stars into the loss cone. Consequently, $n_{\text{b}}(\mathcal{R}, E)$ is determined by the stellar consumption and replenishment processes. Taken these two competing processes into account, CK78 found an orbit-averaged number density by solving the Fokker-Planck equation:

$$n(\mathcal{R}, E) \simeq A(E) \ln \left(\frac{\mathcal{R}}{\mathcal{R}_0} \right) \quad (\mathcal{R} > \mathcal{R}_0), \quad (2)$$

where $A(E)$ is an energy-dependent normalization coefficient and \mathcal{R}_0 is the square of the normalized angular momentum at the zero-boundary below which the number density goes to zero.

Because the square of the normalized angular momentum should be in the range of $\mathcal{R}_0 \leq \mathcal{R} \leq \mathcal{R}_{\text{lc}}$ for stars which will enter inside the tidal disruption radius, the number density for a given E is given by

$$n_{\text{TD}}(E) = \int_{\mathcal{R}_0}^{\mathcal{R}_{\text{lc}}} A_{\text{TD}}(E) \ln \left(\frac{\mathcal{R}}{\mathcal{R}_0} \right) d\mathcal{R}, \quad (3)$$

where the normalization coefficient is estimated to be

$$A_{\text{TD}}(E) = \frac{n_{\text{TD}}(E)}{\mathcal{R}_{\text{lc}} \ln \mathcal{R}_{\text{lc}} - \mathcal{R}_{\text{lc}} \ln \mathcal{R}_0 - \mathcal{R}_{\text{lc}} + \mathcal{R}_0}. \quad (4)$$

By introducing

$$Q \equiv \frac{\Delta \mathcal{R}}{\mathcal{R}_{\text{lc}}}, \quad (5)$$

where $\Delta \mathcal{R}$ is the cumulative change of \mathcal{R} over one orbital period of the star, Magorrian & Tremaine (1999) evaluated \mathcal{R}_0 by

$$\mathcal{R}_0 = g(Q) \mathcal{R}_{\text{lc}}, \quad (6)$$

where

$$g(Q) = \begin{cases} \exp(-Q), & (Q > 1) \\ \exp(-0.186Q - 0.824\sqrt{Q}) & (Q < 1) \end{cases} \quad (7)$$

(see also Merritt 2013). Since \mathcal{R}_0 is very close to \mathcal{R}_{lc} in the case of $Q < 1$, the number density almost goes to zero in the loss cone region. We call the $Q < 1$ case as the empty loss cone regime. On the other hand, \mathcal{R}_0 is smaller than \mathcal{R}_{lc} in the $Q > 1$ case and therefore $R_0 \approx 0$ in the limit of $\mathcal{R}_0 \ll R_{lc}$. We call this limit the full loss cone regime. A significant part of the loss cone region is thus populated with the stars, which are originating from a transition region between the empty and full loss cone regimes. We will explain how to compute Q in Section 3.

2.2. Number density of bound stars

The CK78 solution is solved for the stars moving inside the stellar cusp surrounding an SMBH. Therefore, all of the stars are bound to the SMBH. In this subsection, we first obtain the relation between the orbital eccentricity and the square of the normalized angular momentum, and then we derive the number density for the bound stars in the range of $\mathcal{R} \leq \mathcal{R}_{lc}$.

The specific angular momentum of the bound stars, J , is given by

$$J = \sqrt{GM_{\text{BH}}a(1 - e^2)}, \quad (8)$$

where $e < 1$ and a is the semi-major axis of the star. Putting $e = 0$ into the above equation, we get the circular angular momentum $J_c = \sqrt{GM_{\text{BH}}a}$. At the $e = 1$ limit,

$$J \approx \sqrt{2GM_{\text{BH}}r_p}, \quad (9)$$

where $r_p = a(1 - e)$. Equating r_p with r_t , we get the loss cone angular momentum:

$$J_{lc} = \sqrt{2GM_{\text{BH}}r_t}. \quad (10)$$

Substituting equations (9) and (10) into equation (1), we obtain

$$\mathcal{R} = 1 - e^2 \quad (11)$$

and

$$\mathcal{R}_{\text{lc}} = \frac{2r_t}{a}. \quad (12)$$

Since $n_{\text{TD,b}}(\mathcal{R}, E)d\mathcal{R} = n_{\text{TD,b}}(e, E)de$ due to the mass conservation law, equations (2), (6), and (11) provide the number density of the bound stars in the range of $e_{\text{ll}} \leq e \leq e_{\text{ul}}$:

$$n_{\text{TD,b}}(e, E) = 2A_{\text{TD,b}}(E)e \ln \left(\frac{1 - e^2}{g(Q)\mathcal{R}_{\text{lc}}} \right), \quad (13)$$

where

$$e_{\text{ll}} = \sqrt{1 - 2\frac{r_t}{a}} \quad (14)$$

comes from the $\mathcal{R} = \mathcal{R}_{\text{lc}}$ limit and

$$e_{\text{ul}} = \sqrt{1 - 2g(Q)r_t/a} \quad (15)$$

is obtained by the $\mathcal{R} = \mathcal{R}_0$ limit. Note that $n_{\text{TD,b}}(e, E)$ goes to zero outside of this eccentricity range.

Next, let us obtain the number density of the bound stars as a function of β and E . From equations (9) and (10), r_t and r_p can be expressed as

$$r_p = \frac{J^2}{2GM_{\text{BH}}}, \quad (16)$$

and

$$r_t = \frac{J_{\text{lc}}^2}{2GM_{\text{BH}}}, \quad (17)$$

respectively. Then, we get the relation between β and \mathcal{R} through equation (1)

$$\beta = \frac{\mathcal{R}_{\text{lc}}}{\mathcal{R}} \quad (18)$$

because of $\beta = r_t/r_p$. Since $n_{\text{TD,b}}(\mathcal{R}, E)d\mathcal{R} = n_{\text{TD,b}}(\beta, E)d\beta$ for a given E , we obtain

$$n_{\text{TD,b}}(\beta, E) = \frac{A_{\text{TD,b}}(E)\mathcal{R}_{\text{lc}}}{\beta^2} (-\ln g(Q) - \ln \beta) \quad (19)$$

in the range of $1 \leq \beta \leq 1/g(Q)$, where we used equations (2) and (6) for the derivation.

Note that the number density vanishes to zero at $\beta = 1/g(Q)$, which corresponds to that \mathcal{R} equals \mathcal{R}_0 in the original number density (see equation 2).

2.3. Number density of unbound stars

Most of the theoretical works have so far focused on bound stars within the cusp (Cohn & Kulsrud 1978; Shapiro & Marchant 1978; Magorrian & Tremaine 1999; Wang & Merritt 2004; Stone & Metzger 2016). In this section, we derive the number density of the unbound stars outside of the cusp. The loss cone effect should be negligible at the outside of the influence radius of the SMBH because of $r_t \ll r_h$, so that the stars follow the Maxwellian velocity distribution (we refer this case as the Maxwellian regime in the rest of the paper). In the Maxwellian regime, the number density of the unbound stars is proportional to β^{-2} (Rees 1988):

$$n_{\text{TD,u}}(\beta, E) = A_{\text{TD,u}}(E) \frac{1}{\beta^2}, \quad (20)$$

in the range of $\beta \geq 1$.

Since the pericenter distance is given by $r_p = a(e - 1)$ for the stars on hyperbolic orbits, we obtain

$$e = 1 + \frac{E}{|E_t|} \frac{1}{\beta}, \quad (21)$$

through $E = GM/(2a)$. This equation gives us the number density as a function of only E through $n_{\text{TD,u}}(\beta, E)d\beta = n_{\text{TD,u}}(e, E)de$ as

$$n_{\text{TD,u}}(e, E) = A_{\text{TD,u}}(E) \frac{|E_t|}{E} \quad (22)$$

in the range of $1 < e \leq 1 + r_t/a$. Note that $n_{\text{TD,u}}(e, E) = 0$ if $e > 1 + r_t/a$.

3. N -body experiments

In this section, we test the number density distributions that we have analytically derived by N -body simulations. For comparison purposes, we first compute the simulated

number density as a function of e or β for a given E because of the low resolution. To do so, we integrate equations (13) and (19) over the whole energy range as

$$n_{\text{TD,b}}(e) = \int_{E_t}^0 n_{\text{TD,b}}(e, E) dE, \quad (23)$$

$$n_{\text{TD,b}}(\beta) = \int_{E_t}^0 n_{\text{TD,b}}(\beta, E) dE, \quad (24)$$

where $E_t = -GM_{\text{BH}}/(2r_t)$ is the specific energy estimated at the tidal disruption radius.

For the number densities of the unbound stars, we obtain $n_{\text{TD,u}}(e)$ and $n_{\text{TD,u}}(\beta)$ in the same way but integrate from $E = 0$ to infinity.

There are the following procedures for us to evaluate Q for a given E : First we estimate E at the apocenter distance radius, r_a . Since the number densities of unbound stars are independent of Q (see equations 20 and 22), we do not need to define r_a for the unbound stars. Because $r_a = (1 + e)a \approx 2a$ for the bound stars on very highly eccentric orbits, we obtain $r_a \approx -GM_{\text{BH}}/E$ for a given E . In the case that r_a is larger than the influence radius r_h , we set $r_a \approx r_h$ because the bound stars should be, by definition, inside the r_h .

Next, we compute the averaged change-per-orbit of the angular momentum due to the two-body encounters at for a given r_a as $\langle \Delta J \rangle^2$ because most of the angular momentum of the stars are likely to change at the apocenter passage. This assumption can be justified because the orbiting star passes its apocenter so slowly that has more time to interact with the surrounding stars, and also, the perturbing forces may exert a non-negligible torque to the passing star (Touma & Tremaine 1997; Zhong et al. 2015). From the relaxation theory (Frank & Rees 1976; Merritt 2013), we get

$$\langle \Delta J \rangle^2 \approx J_{\text{K}}(r_a)^2 \left(\frac{t_{\text{dyn}}}{t_{\text{relax}}} \right), \quad (25)$$

where $J_{\text{K}}(r) = \sqrt{GMr}$ is the Keplerian specific angular momentum at r , $t_{\text{dyn}} = r_a/\sigma(r_a)$ is the dynamical timescale,

$$t_{\text{relax}} = \frac{0.065\sigma^3(r_a)}{G^2 m \rho(r_a) \ln \Lambda}. \quad (26)$$

is the local relaxation time (Spitzer 1987), $\sigma(r)$ is the velocity dispersion of the stars, $\rho(r)$ is the radial density profile of the star cluster, $m = M_c/N$ is the mass of the star, and $\ln \Lambda = \ln(0.11N)$ is the Coulomb logarithm (Giersz & Spurzem 1994a). Finally we can evaluate Q from equations (5), (12) and (25) as

$$Q = \frac{\Delta R}{R_{lc}} \approx \left(\frac{t_{\text{dyn}}}{t_{\text{relax}}} \right) \left(\frac{a}{r_t} \right). \quad (27)$$

We find from the above equation that Q is a function of only energy, for the given density profile and velocity dispersion, so that $g(Q)$ becomes thus a function of only E because of equation (7).

3.1. Basic model

We compare the analytically derived number densities with those obtained by N -body simulations. The spherical star cluster consisting of N equal mass stars is initialized with a Plummer model, with an SMBH fixed at the center. The quantities are expressed with the dimensionless Hénon unit, in which $G = M_c = 1$ and the total energy of the system is $E = -1/4$ (Heggie 2014a,b). In the simulations, we take r_t as a fixed accretion radius, in which all the stars are regarded as being tidally disrupted and removed from the simulations. More details can be also seen in Hayasaki et al. (2018). There are two simulation models with $N = 512\text{K}$ and $r_t = 10^{-5}$. In the two models, only the black hole mass is different: While one model has $M_{\text{BH}} = 0.01$, another one has $M_{\text{BH}} = 0.05$. These models are the most-close-to-reality star cluster model in the N -body simulation performed by Hayasaki et al. (2018).

Figure 1 shows the dependence of the number densities on the orbital energy for the stars on both the bound and unbound orbits around the black hole with $M_{\text{BH}} = 0.01$. In each panel, the red histogram shows the simulated number density, while the red line is a

fitted curve by the double broken power-law function. The stars are distributed between E_{\min} (< 0) and E_{\max} (> 0). Note that E_{\min} (roughly -2 in model unit) is much larger than E_t (-500 in model unit). This is consistent with the loss cone theory that the stars are originating far from the tidal disruption radius. We also employ a double broken power-law function to manually fit the simulated number density.

Figure 2 depicts the density profile and the velocity dispersion profile of the star cluster of our models. We use the broken power-law functions to fit these profiles. These functions are used to compute Q of the number densities of the bound stars so that we can extrapolate the density profile and velocity dispersion to the influence radius of the SMBH. It is estimated to be roughly 0.2 in our simulations.

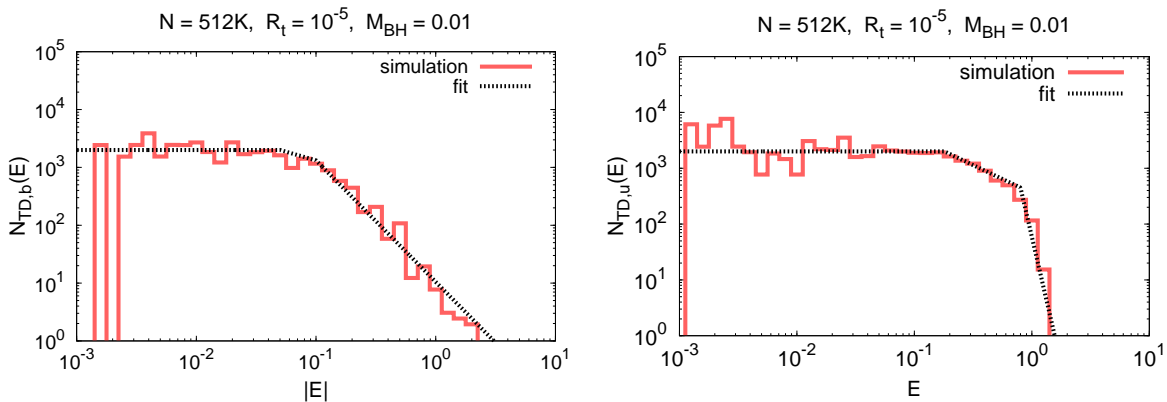


Fig. 1.— Energy dependence of the number densities for both the bound (left panel) and unbound (right panel) stars with $M_{BH} = 0.01$ cases. In each panel, the red histogram shows the simulated number density, while the black dotted line is a fitted curve by the double broken power-law function.

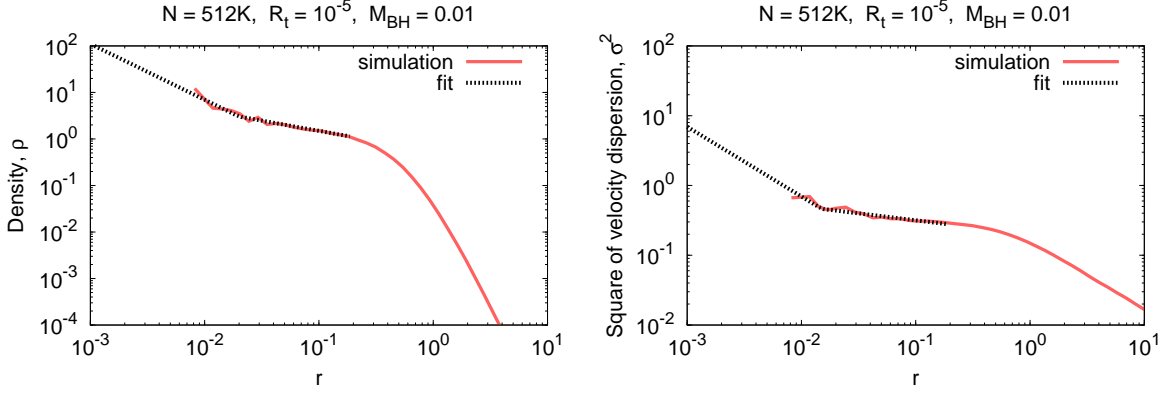


Fig. 2.— Radial profiles of the density and of the square of the stellar velocity dispersion. The black dotted line represents the simulated density profile in left panel, while it shows the square of the simulated stellar velocity dispersion in the right panel. In both panels, the red line represents the fitted curve by the broken power-law function. Note that the red line extends to the influence radius of the SMBH, which corresponds to ~ 0.2 , in each panel.

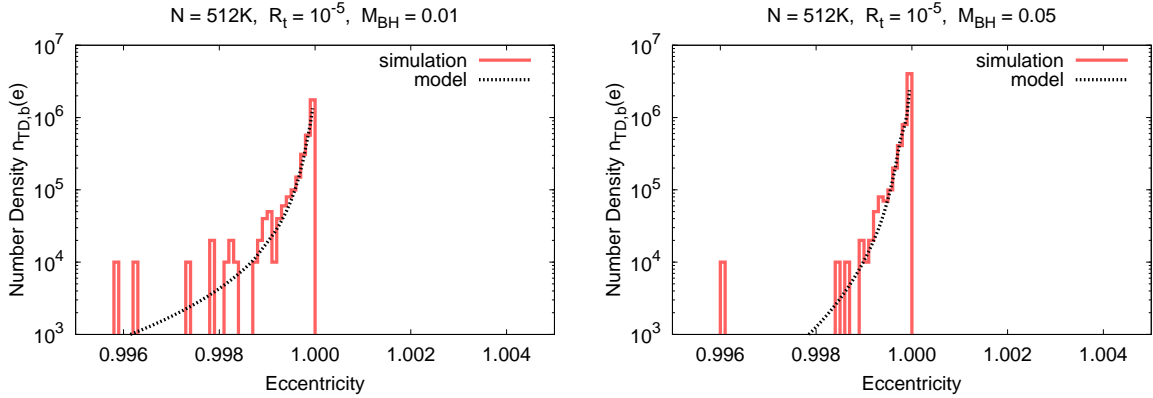


Fig. 3.— Dependence of the number density of the bound stars on the orbital eccentricity. The red histogram and black dotted line represent the simulated and theoretical number densities. The left panel corresponds to $M_{\text{BH}} = 0.01$ case, while the right panel does to $M_{\text{BH}} = 0.05$ case.

3.2. Number densities of the bound stars

We compare the theoretical number densities with the simulated ones. Figure 3 shows the dependence of the number density of the bound stars on the orbital eccentricity. The red histogram and black dotted line represent the simulated and theoretical number densities. In both panels, the simulated number densities are in good agreement with the theoretical ones, except for around 0.998 or the lower eccentricity regime. This deviation of the lower eccentricity regime is mainly caused by a very low particle resolution of the simulations.

The number density of the $M_{\text{BH}} = 0.01$ case is wider for the orbital eccentricity than that of the $M_{\text{BH}} = 0.05$ case. This trend can be interpreted as follows: from equation (14), the lowest eccentricity of the bound stars can be estimated to be $e_{\text{ll}}(M_{\text{BH}}, E_{\text{min}}) = \sqrt{1 - 4r_t|E_{\text{min}}|/GM_{\text{BH}}}$. We find that $E_{\text{min}} = -2$ in the $M_{\text{BH}} = 0.01$ case, whereas $E_{\text{min}} = -4$ (ignoring the isolated bins) in the $M_{\text{BH}} = 0.05$ case. Substituting each quantity into the above equation, we find $e_{\text{ll}}(0.01, -2) = 0.9960$ and $e_{\text{ll}}(0.05, -4) = 0.9984$. These evaluations are consistent with the number density distributions shown in Figure 3.

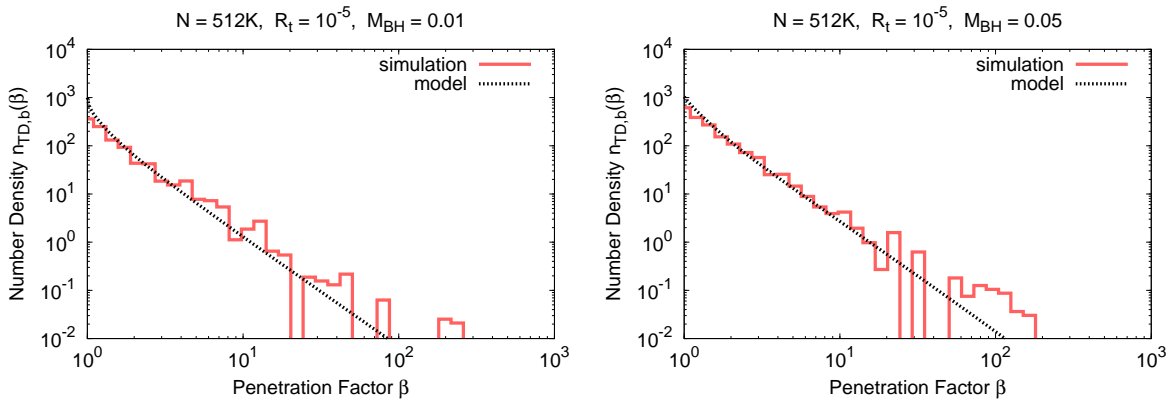


Fig. 4.— β -dependence of the number density of the bound stars. The red histogram and black dotted line represent the simulated and theoretical number densities, respectively. The left panel is the plot of $M_{\text{BH}} = 0.01$ case, while the right panel is that of $M_{\text{BH}} = 0.05$ case.

Figure 4 shows the dependence of the penetration factor on the number density of the bound stars. The figure format of the two panels is the same as Figure 3. We find from the panels that the analytical number densities are in good agreement with the simulated ones within the range of $\beta \lesssim 10$. For $\beta \gtrsim 10$, the deviation between the analytical and simulated number densities gets larger because of the poor resolution regime.

3.3. Number density of the unbound stars

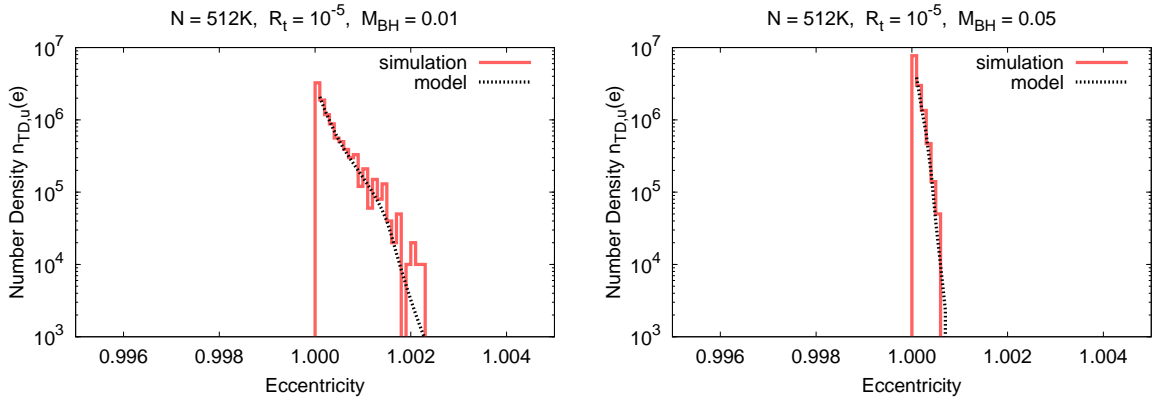


Fig. 5.— Same format as Figure 3 but for the unbound stars.

Figures 5 and 6 compare the analytical number densities of $n_{TD,u}(e)$ and $n_{TD,u}(\beta)$ with those of the simulated number densities. Our theoretical predictions match well with the simulated number densities in both figures. As in the bound star case, the number densities of $M_{BH} = 0.01$ case are more widely distributed over the eccentricity than the $M_{BH} = 0.05$ case. Substituting $a_{\max} = GM_{BH}/(2E_{\max})$ into equation (21) with $\beta = 1$, we obtain $e_{\max}(M_{BH}, E_{\max}) = 1 + 2r_t E_{\max}/(GM_{BH})$. We find from the simulated value of E_{\max} that $e_{\max}(0.01, 1.259) = 1.0025$ and $e_{\max}(0.05, 1.585) = 1.0006$. These suggest that the number density is more widely distributed over the orbital eccentricity in the star cluster with the less massive black hole.

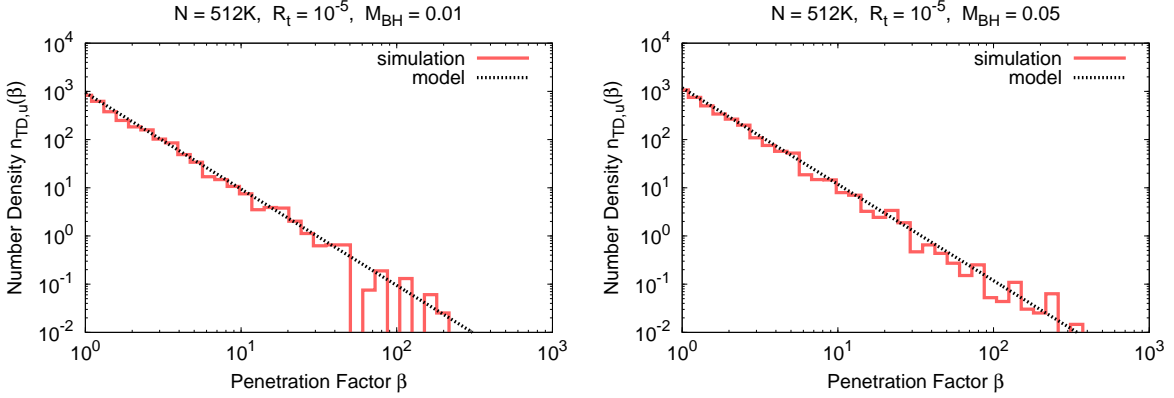


Fig. 6.— Same format as Figure 4 but for the unbound stars.

3.4. Distribution of the stars on the e - β plane

Hayasaki et al. (2018) proposed that there are two critical eccentricities to classify TDEs into five different types by the stellar orbit: eccentric ($e < e_{\text{crit},1}$), marginally eccentric ($e_{\text{crit},1} \lesssim e < 1$), purely parabolic ($e = 1$), marginally hyperbolic ($1 < e < e_{\text{crit},2}$), and hyperbolic ($e \gtrsim e_{\text{crit},2}$) TDEs, respectively, where $e_{\text{crit},1} = 1 - 2(M_{\text{bh}}/m_*)^{-1/3}\beta^{-1}$ and $e_{\text{crit},2} = 1 + 2(M_{\text{bh}}/m_*)^{-1/3}\beta^{-1}$. They found that stars on marginally eccentric and hyperbolic orbits are the main TDE source in a spherical star cluster by N-body experiments. Moreover, these two critical eccentricities have recently modified by taking account of the effect of the penetration factor on the tidal potential as $e_{\text{crit},1} = 1 - 2(M_{\text{bh}}/m_*)^{-1/3}\beta^{k-1}$ and $e_{\text{crit},2} = 1 + 2(M_{\text{bh}}/m_*)^{-1/3}\beta^{k-1}$, where $0 \leq k \lesssim 2$ (Park & Hayasaki 2020). In our simulation case, we find that they are reduced to be $e_{\text{crit},1} = 1 - 2(NM_{\text{bh}})^{-1/3}\beta^{k-1}$ and $e_{\text{crit},2} = 1 + 2(NM_{\text{bh}})^{-1/3}\beta^{k-1}$, respectively. In this section we give new, tighter constraints on the e - β distribution of the stars.

For a given energy $E = -GM_{\text{BH}}/2a$ at the $\mathcal{R} = \mathcal{R}_0$ limit, we can define the minimum

orbital eccentricity of the bound stars by using $r_t/\beta = a(1 - e)$ as

$$e_{\min} = 1 - \frac{2}{\beta} \frac{r_t |E|}{GM_{\text{BH}}}, \quad (28)$$

where $\beta = 1/g(Q)$ is obtained through equations (6) and (18). Adopting $\beta = 1$, we find equation (28) corresponds to equation (14) at $r_t/a \ll 1$: $e_{\text{ll}} = \sqrt{1 - 4r_t|E|/(GM_{\text{BH}})} \approx 1 - 2r_t|E|/(GM_{\text{BH}})$.

For the unbound stars we use another condition that all the unbound stars have $E \leq E_{\max}$. Substituting $a_{\max} = GM_{\text{BH}}/(2E_{\max})$ into equation (21), we obtain

$$e_{\max} = 1 + \frac{2}{\beta} \frac{r_t E_{\max}}{GM_{\text{BH}}}. \quad (29)$$

Adopting $Q = 1$, we obtain the orbital eccentricity on the boundary between the empty loss cone and the full loss cone regimes:

$$e_{\text{lcb}} = 1 - \frac{r_t}{a_{\text{lcb}}\beta}, \quad (30)$$

where the corresponding semi-major axis, a_{lcb} , can be obtained by solving equation (27) with $Q = 1$ semi-analytically. Here, we analytically estimate it as

$$a_{\text{lcb}} = \left(\frac{t_{\text{relax}}}{t_{\text{dyn}}}\right) r_t = \left(\frac{0.13\pi}{\ln \Lambda} \frac{M_{\text{BH}}}{m}\right) r_t \approx 4.1 \times 10^4 r_t \left(\frac{\ln \Lambda}{10}\right)^{-1} \left(\frac{M_{\text{BH}}/m}{10^6}\right) \quad (31)$$

simply by assuming that $\rho(r) = \sigma^2/(2\pi Gr^2)$ and $\sigma = \sqrt{GM/r}$ are the density of the singular isothermal sphere and the Keplerian velocity, respectively (e.g., Merritt 2013). Note also that we adopt $r_a = 2a$ here. In this case, we find $e_{\text{lcb}} \approx 1$ for $\beta \geq 1$.

Figure 7 shows the distribution of the bound and unbound stars, which can cause TDEs, on the e - β plane. The solid blue, solid black, dashed blue lines denote e_{\min} , e_{\max} , and e_{lcb} , respectively. We evaluate these three characteristic eccentricities by using E_{\min} , E_{\max} , and a_{lcb} , which are obtained from our N -body simulations. While the space between e_{lcb} and e_{\min} corresponds to the empty loss cone regime, the space between e_{lcb} and $e = 1$

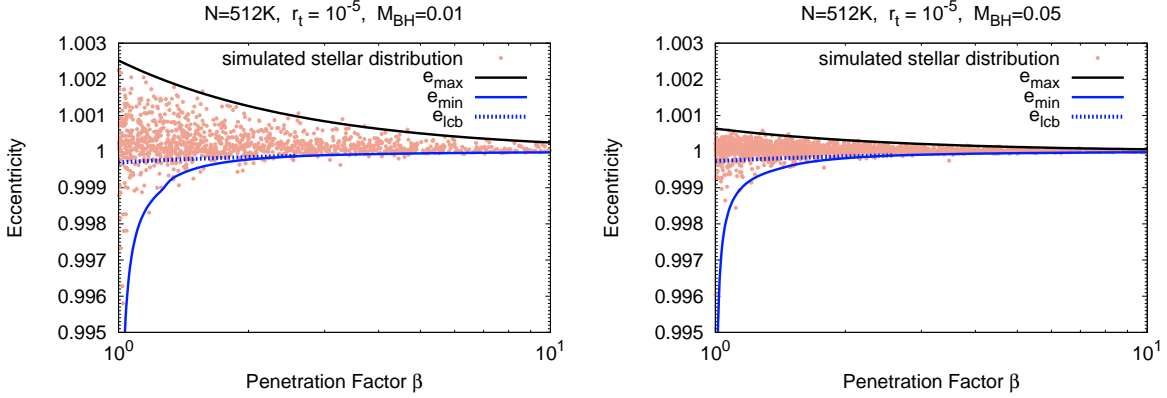


Fig. 7.— Distribution of the stars, which can cause TDEs, on the e - β plane. The solid blue, solid black, dashed blue lines denote e_{\min} , e_{\max} , and e_{lcb} , respectively (see also equations 28-30). Note that $e_{\text{crit},1} \approx 0.885$ and $e_{\text{crit},2} \approx 1.12$ for $M_{\text{bh}} = 0.01$, $\beta = 1$, and $k = 0$ case and $e_{\text{crit},1} \approx 0.933$ and $e_{\text{crit},2} \approx 1.067$ for $M_{\text{bh}} = 0.05$, $\beta = 1$, and $k = 0$ case. Therefore, the two critical eccentricities are much larger or smaller than the current eccentricity scales.

corresponds to the full loss cone regime. The stars located above the $e = 1$ axis are supplied to the black hole from the Maxwellian distribution regime. We find that only a small fraction of the stars are originated from the empty loss cone regime and the corresponding values of β are distributed around unity, whereas most of the stars are originally supplied from the region between e_{lcb} and e_{max} over the much wider range of β . These results are consistent with the loss cone theory: due to the diffusion nature in the empty loss cone regime, the loss cone flux is much smaller than the full loss cone regime, and the stars inside the empty loss cone cannot penetrate the tidal radius too much.

We also find that there are some stars outside e_{\min} or e_{\max} . These outliers seem to violate the loss cone theory. There are two possible reasons for the outliers that unexpectedly behave: first, the more energetic two-body encounter can occur in the N -body simulations, leading to the enhancement of the angular momentum exchange so

that the stars have $\mathcal{R} < \mathcal{R}_0$. Second, the quantity Q depends on the density and the velocity dispersion of the star cluster, which can fluctuate with radius and evolve with time. Therefore we need to reevaluate e_{\min} and e_{\max} by taking account of these effects, but they are beyond the scope of the CK78 solution. Both e_{\min} and e_{\max} are thus likely to deviate from the correct value, producing some outliers on the e - β plane.

4. Discussion

Our analytical models have been tested by N -body simulations in the previous section. Our model can be applied to the observed spherical star cluster systems if we obtain the density and velocity dispersion profile of the star cluster from the observations in addition to the energy distribution of the stars. In this paper, we assumed the energy distribution of the stars because they can be obtained by solving the Fokker-Planck equation in the framework of loss cone theory. We note that we need to consider the effects of the local self-gravitational potential of stars and other potentials such as the galactic potential or the non-dominant SMBH potential in order to handle the unbound stars more precisely.

Let us qualitatively discuss how the number density varies with the black hole mass in the star cluster with the assumption that the density profile of the cusp is $\rho(r) = \rho_h(r/r_h)^{-s}$, where ρ_h is the density at the influence radius. Note that the total stellar mass inside the influence radius equals to the black hole mass. The velocity dispersion inside the influence radius follows $\sigma^2(r) \approx GM_{\text{BH}}/[(1+s)r]$ (Syer & Ulmer 1999). Following Frank & Rees (1976), the critical radius, where the star consumption is balanced with its repopulation, is calculated to be

$$r_{\text{crit}} = \left[\frac{2M_{\text{BH}}^2 r_t N}{15.38(1+s)^2 \ln(0.11N) M_c \rho_h r_h^s} \right]^{\frac{1}{4-s}} \propto M_{\text{BH}}^{\frac{17-3s}{6(4-s)}}, \quad (32)$$

where we use the scaling procedure of Zhong et al. (2014): $r_t \propto M_{\text{BH}}^{1/3}$, $N \propto M_{\text{BH}}$,

$M_c \propto M_{\text{BH}}$, $r_h \propto M_{\text{BH}}^{1/2}$, and $\rho_h \propto M_{\text{BH}}/r_h^3 \propto M_{\text{BH}}^{-1/2}$, and we simply adopt 1/2 for the scaling of r_h instead of 0.54 which is obtained from the $M_{\text{BH}} - \sigma$ relation (Schulze & Gebhardt 2011). Since the ratio of critical to influence radii, r_{crit}/r_h , is proportional to $M_{\text{BH}}^{5/[6(4-s)]}$, it is smaller as the black hole is smaller as long as $s < 4$. In other words, it is expected that the number of the bound stars, which can cause TDEs, increases as the black hole mass decreases. Figure 8 depicts r_{crit}/r_h as a function of M_{BH} (see also equation 32) in the range of $10^3 M_\odot \leq M_{\text{BH}} \leq 10^8 M_\odot$, where we adopt $s = 1.75$ for the Bahcall-Wolf cusp (Bahcall & Wolf 1976) and $s = 1$ for the cusp obtained from the N -body simulations.

Assuming that the semi-major axis a_{min} corresponding to E_{min} is given by a fixed fraction of r_{crit} as $a_{\text{min}} = f r_{\text{crit}}$, where f is a parameter determined by N -body simulations, we have $E_{\text{min}} \propto -M_{\text{BH}}^{\frac{7-3s}{6(4-s)}}$. When $s < 7/3$, E_{min} decreases as M_{BH} decreases. Substituting $E_{\text{min}} = -GM_{\text{BH}}/(2f r_{\text{crit}})$ into equation (28), we obtain

$$e_{\text{min}} = 1 - \frac{1}{\beta} \frac{1}{f} \frac{r_t}{r_{\text{crit}}}. \quad (33)$$

Since the ratio of r_t to r_{crit} is less than 3×10^{-4} over the whole range of the black hole mass, e_{min} is always larger 0.994 for $f = 0.05$ and $\beta = 1$. Because of $1 - e_{\text{min}} \propto r_t/r_{\text{crit}} \propto M_{\text{BH}}^{(s-9)/[6(4-s)]}$, e_{min} is closer to 1 for $s < 4$ as the black hole mass is larger. We also confirm that the black hole mass dependence of the pericenter radius is the same as that of the tidal disruption radius, i.e., $r_{p,\text{min}} = a_{\text{min}}(1 - e_{\text{min}}) \propto M_{\text{BH}}^{1/3} \propto r_t$.

Next, let us see how e_{min} and e_{lcb} (see equations 30 and 33) depends on the black hole mass the e - β plane. The left panel of Figure 9 shows it for the $M_{\text{BH}} = 10^3$ and $10^4 M_\odot$ cases. The e_{lcb} curve of $M_{\text{BH}} = 10^3 M_\odot$ gets larger than $M_{\text{BH}} = 10^4 M_\odot$ case (thick curve). In addition, as mentioned in Section 3.4 (see also Figure 7), most of the bound stars are distributed around the e_{lcb} curve on the plane. These suggest that the star is distributed closer to $e = 1$ over the whole range of β as the black hole mass increases. The right panel of Fig. 9 depicts how the e_{min} curve depends on the black hole mass in the e - β plane. It is clear

from the panel that e_{\min} gets closer to 1 as the black hole mass is larger. This is consistent with that $e_{\min} \propto 1 - M_{\text{BH}}^{(s-9)/[6(4-s)]}$ ($s < 4$) as we estimated in the previous paragraph. In summary, Figure 9 suggests that the stars are supplied into the black hole on extremely marginally eccentric to parabolic orbits for a spherical cluster with $M_{\text{BH}} > 10^7 M_{\odot}$ black hole.

In our N -body simulations, we have adopted a fixed position and mass of the central black hole. For a star cluster with an IMBH, however, the Brownian motion of the black hole modifies the energy distribution of stars so that the number density and e - β distributions can be significantly affected. This is because M_{BH}/m_* of the IMBH system is not so large enough to suppress the Brownian motion. In a forthcoming paper, we will examine how the Brownian motion affects the number density and e - β distributions.

Our analysis of the e - β distributions could provide a good tool to probe the dynamical status of the stars causing TDEs in a star cluster. Hayasaki et al. (2013, 2016) and Bonnerot et al. (2016) studied the accretion disk formation by performing the hydrodynamic simulations, where the authors have adopted $(\beta, e) = (5, 0.8)$ as initial values, although they also used the other combinations of (e, β) . This parameter set is clearly ruled out in our model. However, this does not mean that such a very tightly bound TDE cannot occur. The tightly bound stars are likely to supply to the loss cone not by two-body encounters but by the other mechanisms: the tidal separation of stellar or compact binaries approaching the SMBH (Fragione & Sari 2018), accretion disk mediated TDEs (Kennedy et al. 2016), TDEs produced by a recoiling SMBH (Gualandris & Merritt 2008; Li et al. 2012) or by a merging SMBH binary (Hayasaki & Loeb 2016; Li et al. 2017).

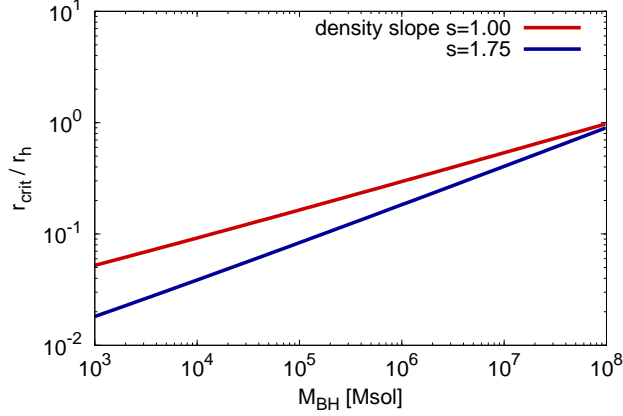


Fig. 8.— Black hole mass dependence of r_{crit}/r_h . The two slopes for the density profiles: $s = 1.75$ (Bahcall-Wolf cusp) and $s = 1$ (N -body simulations) are adopted.

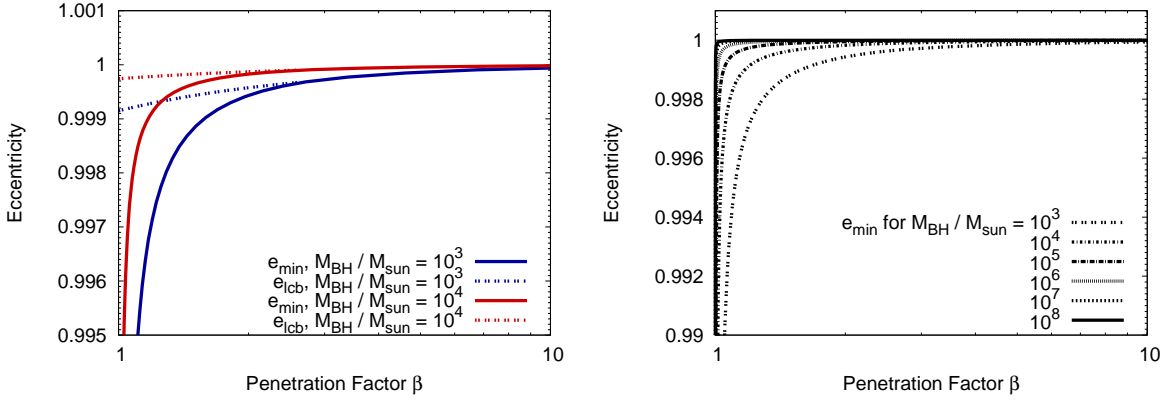


Fig. 9.— Black hole mass dependence of two characteristic eccentricities: e_{min} and e_{lcb} in the e - β plane. We adopt the Bahcall-Wolf density cusp for all the models. The left panel shows β -dependence of e_{min} and e_{lcb} for the $M_{\text{BH}} = 10^3 M_{\odot}$ and $10^4 M_{\odot}$ cases. The dashed lines denote the eccentricity, e_{lcb} , between the empty and full loss cone regimes (see equation 30), whereas the solid lines denote the eccentricity, e_{min} , of most tightly bound stars (see equation 33). The different color shows the different black hole mass. In the right panel, all the lines represent e_{min} . We adopt the different line style for the different black hole mass for $10^3 M_{\odot} \leq M_{\text{BH}} \leq 10^8 M_{\odot}$.

5. Conclusion

Understanding tidal disruption events (TDEs) and their light curves provide a clue to the properties of the central supermassive black hole (SMBH), the accretion disk around it, and to the stellar density and kinematic distributions in the nuclear star cluster surrounding the SMBH. The link between TDEs and central star clusters in galactic nuclei has been a classical subject of seminal papers, such as Frank & Rees (1976); Bahcall & Wolf (1976) finding the classical density distribution near central SMBHs; Dokuchaev & Ozernoi (1977a,b) first noted that accretion and tidal disruption of stars with low angular momentum causes the density profile to flatten out towards the black hole (the energy distribution function $f(E)$ drops towards zero as they showed, today we would call this the empty loss cone region, see also Ozernoi & Reinhardt (1978) for a summary of the topic at the time). CK78 put this on a more quantitative footing by using the technique of solving the orbit-averaged Fokker-Planck equation. Among the classical work in this field also Rees’s conjecture about the fate of tidal debris (Rees 1988) is most noteworthy.

Our study generalizes and expands this by computing approximate distributions of bound and unbound stars in energy-angular momentum space and by transforming the results into density and velocity dispersion profiles. At the same time, we extend the classical Rees’ picture by considering different orbital eccentricities into the tidal disruption radius, which may result - in extreme cases - in 100% mass loss (i.e., hyperbolic TDEs) or 100% accretion of the tidal debris (i.e., eccentric TDEs). Here we follow the work of Hayasaki et al. (2013, 2018) and Park & Hayasaki (2020). By their works, we can improve the understanding of the link between light curves and other TDE characteristics and the stellar distribution of stars in the surrounding nuclear star clusters.

Amaro-Seoane & Spurzem (2001) and Amaro-Seoane et al. (2004) proposed an another model for the loss cone in a spherical star cluster. It is interesting to note that they have

also derived the density and velocity dispersion of bound and unbound loss-cone stars by using moment equations of the basic Fokker-Planck equation and very similar principles to CK78 and this paper. Due to the use of moment equations (so-called gaseous model of star clusters, see e.g. Giersz & Spurzem 1994b) their analysis is completely based on density and velocity profiles rather than orbits with energy and angular momentum. Their model takes into account an anisotropic velocity distribution also for the unbound stars. In the future, a more quantitative comparison of the two models could be done.

We have tested our theoretical models by performing direct N -body simulations; comparison with our analytical model helps to understand the scaling behavior of the N -body simulations since we can still not yet do realistic particle numbers for them. Our primary conclusions are summarized as follows:

1. The number density of the bound stars has been derived as a function of an orbital eccentricity and energy $n(e, E)$ and of a penetration factor and energy $n(\beta, E)$. These two-number densities are given by equations (13) and (19), respectively. For the unbound stars, we have found that $n(\beta, E) \propto 1/\beta^2$ and $n(e, E)$ is a function of only energy, which are given by equations (20) and (22). We have confirmed that the energy integrals of the number densities of both the bound and unbound stars are in good agreement with those obtained by performing N -body simulations.
2. We have also analytically derived the three characteristic orbital eccentricities: e_{\min} , e_{\max} , and e_{lcb} in the loss cone region, where e_{\min} and e_{\max} take the minimum and maximum values for a given β , respectively, whereas e_{lcb} represents the orbital eccentricity which gives the boundary between the empty and full loss cone regimes. These eccentricities are given by equations (28), (29), and (30), respectively. We have confirmed that the stars causing TDEs are distributed between e_{\min} and e_{\max} on the $e - \beta$ plane by N -body experiments. Moreover, we find most of the bound stars are

focused between $e_{\text{lc}}b$ and $e = 1$, i.e., in the full loss cone regime, whereas the remaining bound stars are originating from the empty loss cone regime. This result is consistent with the loss cone theory.

Acknowledgements

S.Z. has been supported by the National Natural Science Foundation of China (NSFC 11603067) and acknowledges the support from Yunnan Astronomical Observatories, Chinese Academic of Sciences. K.H. has been supported by the Korea Astronomy and Space Science Institute (KASI) under the R&D program supervised by the Ministry of Science, ICT and Future Planning, and by the Basic Science Research Program through the National Research Foundation of Korea (NRF) funded by the Ministry of Education (2016R1A5A1013277, 2017R1D1A1B03028580, and 2020R1A2C1007219 (K.H.)). K.H. has been also supported by the National Supercomputing Center with supercomputing resources including technical support (KSC-2019-CRE-0082 (K.H.)). The authors acknowledge the Yukawa Institute for Theoretical Physics (YITP) at Kyoto University. Discussions during the YITP workshop YITP-T-19-07 on International Molecule-type Workshop "Tidal Disruption Events: General Relativistic Transients" were useful to complete this work. The authors also acknowledge support by the Chinese Academy of Sciences (CAS) through the Silk Road Project at NAOC. We are grateful for the support from the Sino-German Center (DFG/NSFC) under grant no. GZ1289. S.L., P.B. and R.S. acknowledge the Strategic Priority Research Program (Pilot B) Multi-wavelength gravitational wave universe of the Chinese Academy of Sciences (No. XDB23040100). P.B. acknowledges the President International Fellowship for Visiting Scientists program of CAS. P.B. and R.S. acknowledge the support of the Volkswagen Foundation under the Trilateral Partnerships grant No. 97778. The work of PB was supported under the special program of the NRF of Ukraine 'Leading and Young

Scientists Research Support' - "Astrophysical Relativistic Galactic Objects (ARGO): life cycle of active nucleus", No. 2020.02/0346.

REFERENCES

- Amaro-Seoane, P., Freitag, M., & Spurzem, R. 2004, *MNRAS*, 352, 655
- Amaro-Seoane, P. & Spurzem, R. 2001, *MNRAS*, 327, 995
- Auchettl, K., Guillochon, J., & Ramirez-Ruiz, E. 2017, *ApJ*, 838, 149
- Bahcall, J. N. & Wolf, R. A. 1976, *ApJ*, 209, 214
- Bonnerot, C., Rossi, E. M., Lodato, G., & Price, D. J. 2016, *MNRAS*, 455, 2253
- Cohn, H. & Kulsrud, R. M. 1978, *ApJ*, 226, 1087
- Dokuchaev, V. I. & Ozernoi, L. M. 1977a, *Zhurnal Eksperimentalnoi i Teoreticheskoi Fiziki*, 73, 1587
- . 1977b, *Pisma v Astronomicheskii Zhurnal*, 3, 295
- Evans, C. R. & Kochanek, C. S. 1989, *ApJ*, 346, L13
- Fragione, G. & Sari, R. 2018, *ApJ*, 852, 51
- Frank, J. & Rees, M. J. 1976, *MNRAS*, 176, 633
- Gezari, S., Chornock, R., Lawrence, A., Rest, A., Jones, D. O., Berger, E., Challis, P. M., & Narayan, G. 2015, *ApJ*, 815, L5
- Gezari, S., Chornock, R., Rest, A., Huber, M. E., Forster, K., Berger, E., Challis, P. J., Neill, J. D., Martin, D. C., Heckman, T., Lawrence, A., Norman, C., Narayan, G., Foley, R. J., Marion, G. H., Scolnic, D., Chomiuk, L., Soderberg, A., Smith, K., Kirshner, R. P., Riess, A. G., Smartt, S. J., Stubbs, C. W., Tonry, J. L., Wood-Vasey, W. M., Burgett, W. S., Chambers, K. C., Grav, T., Heasley, J. N.,

- Kaiser, N., Kudritzki, R.-P., Magnier, E. A., Morgan, J. S., & Price, P. A. 2012, *Nature*, 485, 217
- Giersz, M. & Spurzem, R. 1994a, *MNRAS*, 269, 241
- . 1994b, *MNRAS*, 269, 241
- Gualandris, A. & Merritt, D. 2008, *ApJ*, 678, 780
- Guillochon, J. & Ramirez-Ruiz, E. 2013, *ApJ*, 767, 25
- Hayasaki, K. & Loeb, A. 2016, *Scientific Reports*, 6, 35629
- Hayasaki, K., Stone, N., & Loeb, A. 2013, *MNRAS*, 434, 909
- . 2016, *MNRAS*, 461, 3760
- Hayasaki, K., Zhong, S., Li, S., Berczik, P., & Spurzem, R. 2018, *ApJ*, 855, 129
- Heggie, D. C. 2014a, *ArXiv e-prints*
- . 2014b, *MNRAS*, 445, 3435
- Hills, J. G. 1975, *Nature*, 254, 295
- Holoien, T. W. S., Kochanek, C. S., Prieto, J. L., Stanek, K. Z., Dong, S., Shappee, B. J., Grupe, D., Brown, J. S., Basu, U., Beacom, J. F., Bersier, D., Brimacombe, J., Danilet, A. B., Falco, E., Guo, Z., Jose, J., Herczeg, G. J., Long, F., Pojmanski, G., Simonian, G. V., Szczygieł, D. M., Thompson, T. A., Thorstensen, J. R., Wagner, R. M., & Woźniak, P. R. 2016, *MNRAS*, 455, 2918
- Holoien, T. W.-S., Prieto, J. L., Bersier, D., Kochanek, C. S., Stanek, K. Z., Shappee, B. J., Grupe, D., Basu, U., Beacom, J. F., Brimacombe, J., Brown, J. S., Davis, A. B., Jencson, J., Pojmanski, G., & Szczygieł, D. M. 2014, *MNRAS*, 445, 3263

Hung, T., Gezari, S., Blagorodnova, N., Roth, N., Cenko, S. B., Kulkarni, S. R., Horesh, A., Arcavi, I., McCully, C., Yan, L., Lunnan, R., Fremling, C., Cao, Y., Nugent, P. E., & Wozniak, P. 2017, *ApJ*, 842, 29

Kennedy, G. F., Meiron, Y., Shukirgaliyev, B., Panamarev, T., Berczik, P., Just, A., & Spurzem, R. 2016, *MNRAS*, 460, 240

Li, S., Liu, F. K., Berczik, P., Chen, X., & Spurzem, R. 2012, *ApJ*, 748, 65

Li, S., Liu, F. K., Berczik, P., & Spurzem, R. 2017, *ApJ*, 834, 195

Lodato, G., King, A. R., & Pringle, J. E. 2009, *MNRAS*, 392, 332

Lodato, G. & Rossi, E. M. 2011, *MNRAS*, 410, 359

MacLeod, M., Guillochon, J., & Ramirez-Ruiz, E. 2012, *ApJ*, 757, 134

Magorrian, J. & Tremaine, S. 1999, *MNRAS*, 309, 447

Merritt, D. 2013, *Classical and Quantum Gravity*, 30, 244005

Miller, J. M., Kaastra, J. S., Miller, M. C., Reynolds, M. T., Brown, G., Cenko, S. B., Drake, J. J., Gezari, S., Guillochon, J., Gultekin, K., Irwin, J., Levan, A., Maitra, D., Maksym, W. P., Mushotzky, R., O'Brien, P., Paerels, F., de Plaa, J., Ramirez-Ruiz, E., Strohmayer, T., & Tanvir, N. 2015, *Nature*, 526, 542

Mummery, A. & Balbus, S. A. 2020, *MNRAS*, 492, 5655

Ozernoi, L. M. & Reinhardt, M. 1978, *Ap&SS*, 59, 171

Park, G. & Hayasaki, K. 2020, *ApJ*, 900, 3

Phinney, E. S. 1989, in *IAU Symposium, Vol. 136, The Center of the Galaxy*, ed. M. Morris,

Rees, M. J. 1988, *Nature*, 333, 523

Schulze, A. & Gebhardt, K. 2011, *ApJ*, 729, 21

Shapiro, S. L. & Marchant, A. B. 1978, *ApJ*, 225, 603

Spitzer, L. 1987, *Dynamical evolution of globular clusters*

Stone, N. C. & Metzger, B. D. 2016, *MNRAS*, 455, 859

Strubbe, L. E. & Quataert, E. 2009, *MNRAS*, 400, 2070

Syer, D. & Ulmer, A. 1999, *MNRAS*, 306, 35

Touma, J. & Tremaine, S. 1997, *MNRAS*, 292, 905

van Velzen, S., Stone, N. C., Metzger, B. D., Gezari, S., Brown, T. M., & Fruchter, A. S.
2019, *ApJ*, 878, 82

Wang, J. & Merritt, D. 2004, *ApJ*, 600, 149

Zhong, S., Berczik, P., & Spurzem, R. 2014, *ApJ*, 792, 137

—. 2015, *ApJ*, 811, 22